crystals

MDPI

Article

Synthesis, Crystal Structures, and Magnetic Properties of Three Cobalt(II) Coordination Polymers Constructed from 3,5-Pyridinedicarboxylic Acid or 3,4-Pyridinedicarboxylic Acid Ligands

Xiaojing Zhou [1,*], Xiaolei Guo [2], Lili Liu [1], Zhan Shi [2], Yan Pang [1] and Xishi Tai [1,*]

[1] School of Chemical & Chemical Engineering and Environmental Engineering, Weifang University, Weifang 261061, China; liulili122@126.com (L.L.); wfpangy@163.com (Y.P.)

[2] State Key Laboratory of Inorganic Synthesis & Preparative Chemistry, College of Chemistry, Jilin University, Changchun 130012, China; angle52mm@163.com (X.G); zshi@mail.jlu.edu.cn (Z.S.)

* Correspondence: zhouxiaojing105@163.com (X.Z.); taixs@wfu.edu.cn (X.T.)

Received: 27 January 2019; Accepted: 18 March 2019; Published: 21 March 2019

Abstract: Three 2D new coordination polymers $Co_2(L_1)_2$(1,10-Phenanthroline)$_2$(DMF)$_{0.5}$(H_2O) (**1**), (H_2L_1 = Pyridine-3,5-dicarboxylic acid) Co(L_1)(2,2-bipyridine) (**2**), and Co(L_2)(2,2-bipyridine) (DMF) (**3**) (H_2L_2 = Pyridine-3,4-dicarboxylic acid) were synthesized through a solvothermal reaction of cobalt nitrate and pyridine carboxylic acid ligand with the auxiliary ligand (1,10-Phenanthroline or 2,2-bipyridine). They were characterized by X-ray diffraction and elemental analysis, infrared spectroscopy, thermogravimetry analysis, and magnetism. Compounds **1**–**3** featured 2D hexagonal (6,3) networks which linked into 3D supramolecular architectures through π–π interaction. In addition, compounds **1** and **2** showed the antiferromagnetic exchange interactions, and the magnetic property of compound **3** exhibited ferromagnetic exchange interactions.

Keywords: solvothermal synthesis; coordination polymers; pyridine carboxylic acid; magnetism properties

1. Introduction

The rational design and synthesis of coordination polymers have been under intensive investigation in the past two decades because of their potential applications in a number of fields, such as in the areas of storage, separation, catalysis, magnetism, and luminescence [1–9]. However, the reasonable synthesis and design of such target materials are still a great challenge in crystal engineering. There are many factors that can influence the final structures of coordination polymers, such as metal ions, ligands, metal-to-ligand ratio, solvent system, pH, etc., and among these factors, the selection of suitable organic ligands plays a crucial rule in the constructions of fascinating coordination polymers [10–12]. Just like the reported structures, it is a convenient strategy to construct coordination polymers with a single ligand containing N or O donor atoms [13,14]. Nevertheless, for the purpose of getting more coordination polymers with novel structures and excellent properties, single coordination atoms sometimes cannot meet the needs of researchers. Therefore, much attention has been paid to organic ligands containing various coordination atoms, of which pyridylcarboxylates are one variety. Accordingly, many works have been conducted to construct coordination polymers with different structures using pyridine carboxylic acid ligands, and various extended structures have been successfully constructed with different metal ions, for instance, six novel 3D coordination polymers with interesting topologies were synthesized by Zhu with pyridine-3,4-dicarboxylic acid [15], and a series of Ln coordination polymers with photoluminescent properties were constructed based on

pyridine-3,5-dicarboxylic acid [16–22]. Taking into account the reported works, in this paper we chose the symmetrical pyridine-3,5-dicarboxylic acid and asymmetrical pyridine-3,4-dicarboxylic acid as the ligands because these two ligands can be deprotonated to form HL^- and L^{2-} anions which have the flexible and versatile coordination modes to bridge metal ions. Furthermore, the π-electric conjugated system of the pyridine dicarboxylic acid and auxiliary ligands (1,10-Phenanthroline and 2,2-bipyridine) are beneficial for the formation of stable supramolecular structures [15,21–23]. Meanwhile we chose cobalt nitrate as the metal source, and thus they could form both discrete and consecutive new Co compounds with magnetic behavior, having potential applications in magnetic materials [24,25].

In this contribution, three new 2D coordination polymers—$Co_2(L_1)_2$(1,10-Phenanthroline)$(DMF)_{0.5}(H_2O)$ (**1**), $Co(L_1)$(2,2-bipyridine) (**2**), and $Co(L_2)$(2,2-bipyridine)(DMF) (**3**)—were isolated under solvothermal conditions and characterized by single-crystal X-ray diffraction analysis, elemental analysis, infrared (IR) spectroscopy, and thermogravimetry analysis (TGA), and the magnetic susceptibilities were also investigated.

2. Materials and Methods

2.1. Materials and Physical Measurements

All reagents and solvents used in the experiment were obtained directly from a commercial source, and used without further purification. Inductively coupled plasma (ICP) analysis of Co and elemental analysis were performed on a Perkin-Elmer Optima 3300DV Spectrometer and a Perkin-Elmer 2400 element analyzer, respectively. Infrared (IR) spectra were recorded on a Nicolet Impact 410 FTIR spectrometer using a KBr pellet in the range of 4000–400 cm^{-1}. Powder X-ray diffraction (PXRD) measurements were executed by using a Rigaku D/max 2550 X-Ray Powder Diffractometer. Thermogravimetric analysis was performed with a TGA Q500 V20.10 Build 36 instrument with a heating rate of 10 °C/min in a flowing N_2 atmosphere. Magnetic susceptibility data were obtained by SQUID magnetometer (Quantum MPMS) in the range of 2–300 K using an applied field of 1000 Oe.

2.2. Methods

2.2.1. Synthesis of $\{Co_2(L_1)_2$(1,10-Phenanthroline$)_2\}(DMF)_{0.5}(H_2O)$ (**1**)

H_2L_1 (0.05 mmol, 8.356 mg), $Co(NO_3)_2{\cdot}6H_2O$ (0.1 mmol, 29.1 mg), and 1,10-Phenanthroline (0.1 mmol, 18 mg) were dissolved in DMF (5 mL), then the solution was transferred and sealed in a 15 mL Teflon-lined stainless steel autoclave, and heated at autogenous pressure at 120 °C for 3 days, followed by slow cooling (10 °C·h^{-1}) to room temperature. The resulting mixture was washed by DMF, yielding purple block crystals and dried in the air. Yield for compound **1**: 65%. IR (KBr disc, cm^{-1}) 3449 (m), 3056 (w), 2359 (w), 1617 (s), 1571 (s), 1514 (m), 1359 (s), 1275 (m), 1120 (w), 1093 (m), 842 (s), 765 (s), 720 (s), 680 (s), 565 (w), 442 (w). Elemental analysis (%): Calcd for: $C_{39.5}H_{27.5}Co_2N_{6.5}O_{9.5}$: Co 13.65 C 54.94 H 3.21 N 10.54; found: Co 13.49 C 55.03 H 3.26 N 10.52.

2.2.2. Synthesis of $Co(L_1)$(2,2-bipyridine) (**2**)

H_2L_1 (0.05 mmol, 8.356 mg), $Co(NO_3)_2{\cdot}6H_2O$ (0.1 mmol, 29.1 mg), and 2,2-bipyridine (0.1 mmol, 18 mg) were dissolved in DMF (5 mL), then the solution was transferred to a 15 mL Teflon-lined stainless autoclave, which was heated to 120 °C for 3 days, followed by slow cooling (10 °C·h^{-1}) to room temperature. The resulting mixture was washed by DMF, then the purple block crystals were collected and air-dried. Yield for compound **2**: 65%. IR (KBr disc, cm^{-1}) 3449 (m), 3056 (w), 2359 (w), 1617 (s), 1571 (s), 1514 (m), 1359 (s), 1275 (m), 1120 (w), 1093 (m), 842 (s), 765 (s), 720 (s), 680 (s), 565 (w), 442 (w). Elemental analysis (%): Calcd for: Co 15.5 $C_{38}H_{22}Co_2N_6O_8$: C 56.4 H 2.72 N 10.4; found: Co 15.45 C 56.61 H 2.83 N 10.36.

2.2.3. Synthesis of Co(L_2)(2,2-bipyridine)(DMF) (**3**)

The mixture of $Co(NO_3)_2 \cdot 6H_2O$ (0.1 mmol, 29.1 mg), H_2L_2 (0.05 mmol, 8.356 mg), 2,2-bipyridine (0.2 mmol, 31.2 mg), DMF(3 mL), CH_3CH_2OH (2 mL), and H_2O (1 mL) were transferred to a 15 mL Teflon-lined stainless steel autoclave, and heated at 100 °C for 3 days, followed by slow cooling (10 °C·h^{-1}) to room temperature. The resulting mixture was washed by DMF, and purple columnar crystals were collected and air-dried (yield 42%). IR (KBr disc, cm^{-1}) 3449 (m), 3095 (w), 3056 (w), 1972 (w), 1623 (s), 1559 (s), 1436 (m), 1404 (m), 1378 (s), 1294 (w), 1165 (w), 1062 (w), 875 (m), 842 (m), 765 (s), 733 (m), 675 (m), 604 (w), 572 (w), 456 (w). Elemental analysis (%): Calcd for: $C_{20}H_{18}CoN_4O_5$: Co 13.0 C 53.0 H 4.0 N 12.36; found: Co 13.16 C 53.06 H 3.98 N 12.47.

2.3. Crystal Structural Determination

Single crystal X-ray diffraction data for compounds **1–3** were obtained using a Rigaku RAXIS-RAPID equipped with graphite-monochromated Mo Kα radiation (λ = 0.71073 Å) at 293 K. The data processing was accomplished with the PROCESS-AUTO processing program. The structures were solved with the direct methods of the SHELXL crystallographic software package and refined on F^2 by full-matrix least square techniques. All non-hydrogen atoms of the three compounds were refined with anisotropic thermal parameters. All hydrogen atoms of the organic molecule were geometrically placed and added to the structure factor calculation. Crystal data and structure refinement details of compounds **1–3** are summarized in Table 1. Crystallographic data for the structures reported in this paper have been deposited in the Cambridge Crystallographic Data Centre (CCDC), and the CCDC numbers of the three compounds are CCDC-1876151 (**1**), CCDC-1876152 (**2**), and CCDC-1876153 (**3**). As for the molecular formula of compounds **1** and **3**, it is difficult to obtain the exact solvent molecules in the structure, so we further determined these using Elemental analysis, TGA and Platon program, and the solvent composition (compound **1**: 0.5DMF + H_2O; compound **2**: DMF) was calculated from the TGA and elemental analysis that were in agreement with the data from Platon program [26].

Table 1. Crystallographic data for compounds **1–3**.

Compound	1	2	3
Empirical formula	$C_{39.5}H_{27.5}Co_2N_{6.5}O_{9.5}$	$C_{17}H_{11}CoN_3O_4$	$C_{20}H_{18}CoN_4O_5$
Formula weight	863.48	380.22	453.31
Temperature/K	293 (2)	293 (2)	293 (2)
Crystal system	Monoclinic	Orthorhombic	Monoclinic
Space group	$P2_1/n$	$P2_12_12_1$	$P1n1$
a/nm	18.8708(10)	9.1422(6)	7.6625(6)
b/nm	9.7415(5)	9.9771(6)	9.3679(8)
c/nm	19.5268(11)	18.2000	10.4560(8)
α	90	90	90
β	92.669(2)	90	95.700(3)
γ	90	90	90
V/Å^3	3585.7(3)	1660.07(18)	746.84(10)
Z	4	4	2
D_c (Mg·m^{-3})	1.498	1.521	1.691
F(000)	1640	772	386
GOF	1.023	1.044	1.006
R_1[a]/wR_2[b] $I > 2\sigma(I)$	R_1 = 0.0557 wR_2 = 0.1066	R_1 = 0.0289 wR_2 = 0.0636	R_1 = 0.0320 wR_2 = 0.0570
R_1/wR_2 (all data)	R_1 = 0.0987 wR_2 = 0.1201	R_1 = 0.0340 wR_2 = 0.0655	R_1 = 0.0426 wR_2 = 0.0597

[a] $R_1 = ||F_o| - |F_c||/\Sigma|F|_o$. [b] $wR_2 = [\Sigma w(F_o^2 - F_c^2)^2/\Sigma w(F_o^2)^2]^{1/2}$. w = $1/[\sigma^2(F_o^2) + (ap)^2 + (bp)]$, p = [max($F_o^2$ or 0) + 2(F_c^2)]/3.

3. Results and Discussion

*3.1. Crystal Structures of $Co_2(L_1)_2$(1,10-Phenanthroline)$_2(DMF)_{0.5}(H_2O)$ (**1**)*

Compound **1** crystallizes in the monoclinic space group $P2_1/n$. The asymmetric unit of **1** contains two Co(II) atoms, two L_1 ligands, and two 1,10-Phenanthroline molecules. 1,10-Phenanthroline molecule (Figure S1 in the supplementary materials). The Co atom is hexacoordinated, adopting $[CoN_3O_3]$ distorted octahedron geometry coordination environments. Each Co atom is coordinated with one O atom from one L_1 ligand, two O atoms from one $L_{1'}$ ligand in bidentate coordinated mode, one N atom from one L_1 ligand, and two N atoms from one 1,10-Phenanthroline molecule (Figures S1 and S2). Accordingly, the Co–O and Co–N bond lengths are 2.000 Å−2.417 Å and 2.097−2.165 Å, respectively. The Co–O and Co–N distances are quite similar to the normal Co–O and Co–N distances [27–31]. In compound **1**, the L_1 ligand shows two types of coordination modes. In addition, L_{1a} adopts a μ_2–η^1:η^1 bridging coordination mode to connect three Co ions with the Co···Co separations of 0.7402 nm, 0.9902 nm, and 1.031 nm. Meanwhile, L_{1b} adopts the μ^4–η^1:η^1:η^1:η^1 coordination mode to connect three Co ions with the Co···Co separations of 0.9639 nm, 0.9874 nm, and 1.031 nm (Figure S2). Compound **1** features a 2D hexagonal (6,3) layer with hcb topology, where both L_1 and $L_{1'}$ act as tri-connected nodes, and the auxiliary ligand occupies two reaction sites of the distorted octahedron. As a result, the hexacoordinated Co atom provides a tri-connected node (Figure 1a,b) [32–35]. Furthermore, the 2D layers are extended into a 3D supramolecular architecture by π–π interactions between the 1,10-Phenanthroline molecules with center-to-center distances of 3.34−3.45 Å (Figure S7) [36–40].

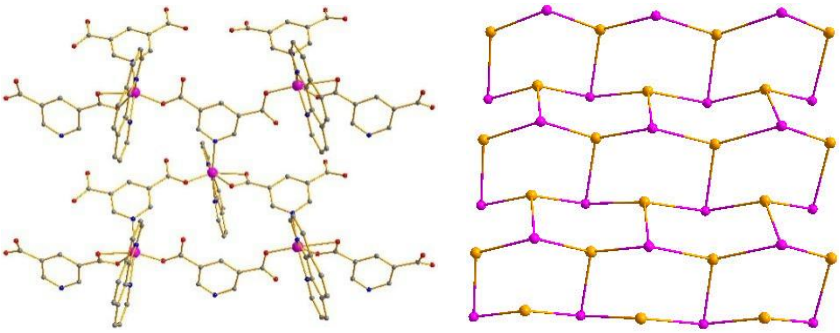

(**a**) (**b**)

Figure 1. (**a**) 2D network of compound **1**. (**b**) Topology of compound **1**.

*3.2. Crystal Structures of Co(L_1)(2,2-bipyridine) (**2**)*

Compound **2** crystallizes in the orthorhombic system with the $P2_12_12_1$ space group. The asymmetric unit of crystal **2** consists of one Co atom, one L_1 ligand, and one 2,2-bypyridine. As depicted in Figure 2a, the Co center adopts a distorted heptacoordinated pentagonal bipyramid configuration through the coordination of three nitrogen atoms from one 2,2-bypyridine and one L_1 ligand, and four oxygen atoms from two individual L_1 ligands in a chelating mode (Figures S3 and S4). The Co–O (Co–O = 2.0642 Å−2.7512 Å) and Co–N (Co–N = 2.1052 Å−2.1340 Å) distances are quite similar to the normal ranges [27–31]. The L_1 ligand adopts a bidentate coordination mode and utilizes one nitrogen atom to connect three Co atoms with the Co···Co separations of 0.7395 nm, 0.7714 nm, and 0.9977 nm. The neighboring three Co atoms are bridged by six L_1 ligands into a 2D hexagonal (6,3) network (Figure 2a) with hcb topology (Figure 2b) [32–35]. Furthermore, the adjacent layers are further linked into a 3D supramolecular architecture by π–π interactions between the 2,2-bipyridine molecules with center-to-center distances of 3.66−3.80 Å (Figure S8) [36–40].

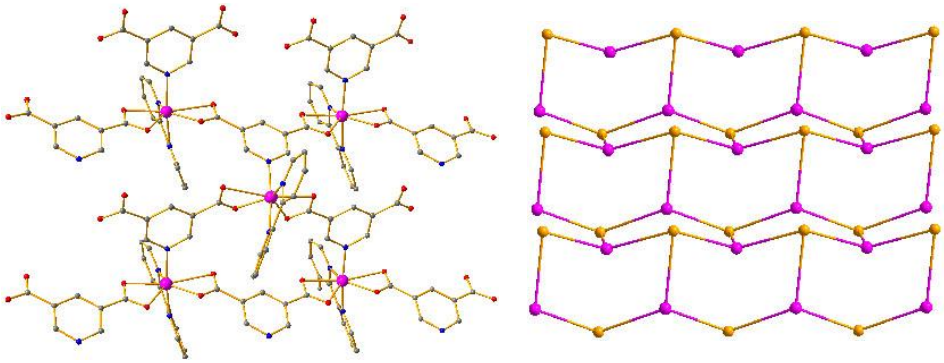

(**a**) (**b**)

Figure 2. (**a**) 2D network of compound **2**. (**b**) Topology of compound **2**.

*3.3. Crystal Structures of Co(L_2)(2,2-bipyridine)(DMF) (**3**)*

Compound **3** crystallizes in the monoclinic system with the *P*1*n*1 space group. The asymmetric unit of compound **3** contains a crystallographically independent Co atom, a L_1 ligand, and a 2,2-bipyridine molecule. As depicted in Figure 3a, the Co atom is hexacoordinated, adopting [CoN_3O_3] distorted octahedron geometry coordination environments. Each Co atom is coordinated with three oxygen atoms of two different L_2 ligands, three nitrogen atoms from one 2,2-bipyridine, and one L_2 ligand (Figure S5). Accordingly, Co−O and Co−N bond lengths are 2.000 Å−2.2275 Å and 2.088−2.172 Å, respectively, which are acceptable bond lengths [27–31]. The L_2 ligand adopts a chelate-monodentate coordination and utilizes one nitrogen atom to connect three Co atoms with the Co···Co separations of 0.7642 nm, 0.7662 nm, and 0.8146 nm (Figure S6). The neighboring three Co atoms are bridged by six other L_2 ligands into a 2D hexagonal (6,3) network (Figure 3a) with hcb topology (Figure 3b) [32–35]. Furthermore, the adjacent layers are further linked into a 3D supramolecular architecture by π–π interactions between the 2,2-bipyridine molecules with center-to-center distances of 3.56–3.92 Å (Figure S9) [36–40].

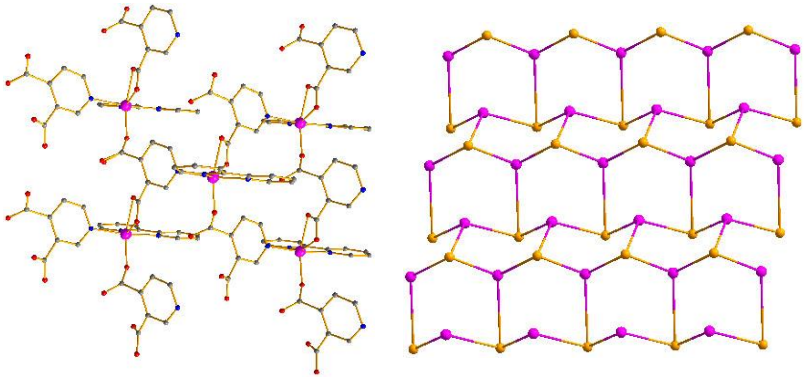

(**a**) (**b**)

Figure 3. (**a**) 2D network of compound **3**. (**b**) Topology of compound **3**.

3.4. X-Ray Power Diffraction Analysis and Thermal Analysis

The diffraction peaks of compounds **1**–**3** were confirmed with good agreement between the experimental (black line) and simulated PXRD patterns (red line) (Figures S10–S12), and the phenomenon indicates that the synthesized compounds **1**–**3** have good phase purity.

The thermal stability of compounds **1**–**3** were examined by TG analysis in the range of 25−800 °C, and the results are given in Figure 4. For **1**, this led to weight loss from 135 to 378 °C as uncoordinated

water and DMF molecules were separated from the framework (Obsd. 6.26%, Calcd. 6.3%), and further loss resulted from the decomposition of organic components. Finally, a residue of Co−O was left. For **2**, the framework started to decompose from 338 to 800 °C, and Co−O was the final residue. In terms of **3**, weight loss occurred at 141−400 °C because of the removal of uncoordinated DMF molecules in the framework (Obsd. 16.3%, Calcd. 16.14%), and the decomposition of the framework occurred at 220 °C, so a residue of CoO remained.

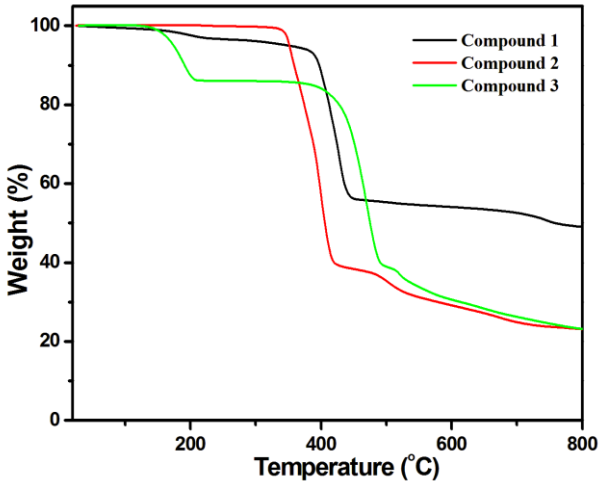

Figure 4. Thermogravimetric analysis for compounds **1**–**3**.

3.5. Magnetic Properties

When the magnetic field was 1000 Oe and the temperature was in the range of 2–300 K, the variable temperature magnetic susceptibility of compounds **1–3** was measured. The curves of $\chi_M T$ and $\chi_M{}^{-1}$ vs. T of compounds **1**–**3** are presented in Figure 5, Figure 6, and Figure 7, respectively. The $\chi_M T$ value of compound **1** at 300 K was 5.60 emu·K mol^{-1} for a Co^2 unit, where the value was much higher than the theoretical $\chi_M T$ value of the spin-only one for two isolated Co^{2+} ions (3.75 emu·K mol^{-1} and S = 3/2), which is mainly due to the spin-orbit coupling of the high-spin Co^{2+} ions. Upon the temperature cooling to 50 K, the $\chi_M T$ value was kept roughly constant. Nevertheless, it decreased suddenly and gave the $\chi_M T$ value 3.07 emu·K mol^{-1} at 2 K. The sudden decrease below 50 K was due to the antiferromagnetic coupling between the paramagnetic centers and the zero-field splitting (Figure 5). The $\chi_M T$ value of compound **2** at 300 K was 2.79 emu·K mol^{-1} for a Co ion, where the value was much higher than the theoretical $\chi_M T$ value of the spin-only one for one isolated Co^{2+} ion (1.875 emu·K mol^{-1} and S = 3/2), but it still fell within the usual range for octahedral Co^{2+} ions in the 4T2g state. Upon the temperature cooling to 50 K, the $\chi_M T$ value was kept roughly constant. The phenomenon is reminiscent of antiferromagnetic behavior (Figure 6). The $\chi_M T$ value of compound **3** at 300 K was 2.23 emu·K mol^{-1} for a Co ion, where the value was much higher than the theoretical $\chi_M T$ value for one isolated Co^{2+} ion (1.875 emu·K mol^{-1} and S = 3/2), though it fell within the usual range for octahedral Co^{2+} ions in the 4T2g state. The $\chi_M T$ value was kept roughly constant until the temperature decreased to 50 K, suggesting a ferromagnetic interaction between Co ions (Figure 7). Curie−Weiss law was used to fit the $\chi_M{}^{-1}$ data from 2–300 K, acquiring $\theta = -1.77$ K, C = 5.67 emu·K mol^{-1} for compound **1**. The negative θ value and $\chi_M T$ trend with temperature fully demonstrated an antiferromagnetic effect of compound **1**. In compound **2**, the parameters C = 1.0 emu·K mol^{-1} and $\theta = 0$ K indicated an antiferromagnetic effect of compound **2**, while in compound **3**, giving C = 2.2 emu·K mol^{-1} and $\theta = 6.5$ K, a ferromagnetic effect was suggested between the Co^{2+} ions (Table 2) [24,25].

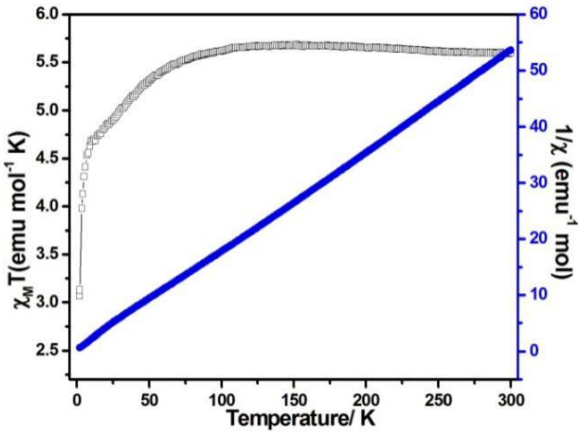

Figure 5. χ_MT vs. T (filled triangles) and $\chi_M{}^{-1}$ (filled squares) plots for compound **1** at 0.1 T.

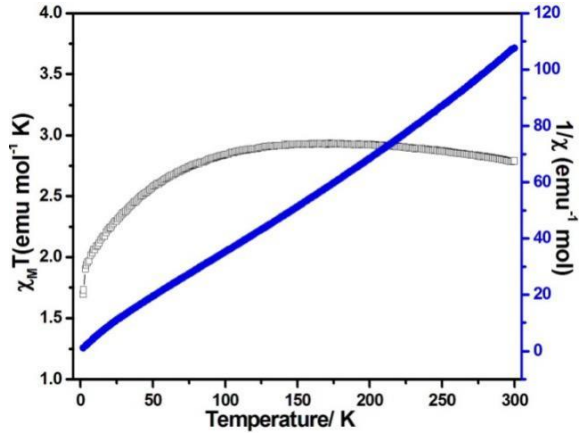

Figure 6. χ_MT vs. T (filled triangles) and $\chi_M{}^{-1}$ (filled squares) plots for compound **2** at 0.1 T.

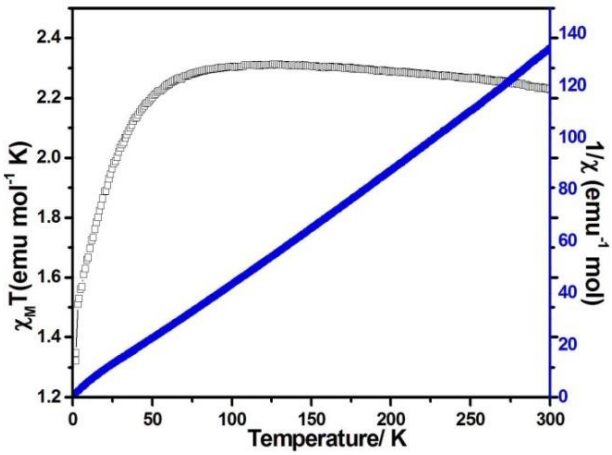

Figure 7. χ_MT vs. T (filled triangles) and $\chi_M{}^{-1}$ (filled squares) plots for compound **3** at 0.1 T.

Table 2. Magnetic susceptibility of compounds **1**–**3**.

Compound	1	2	3
X_mT/emu·K mol^{-1}	5.6	2.79	2.23
C/emu·K mol^{-1}	5.67	1.0	2.2
θ/K	−1.77	0	6.5

4. Conclusions

Three 2D coordination polymers were prepared based on cobalt nitrate and H_2L_1, H_2L_2 ligands. Compounds **1**–**3** all featured 2D hexagonal (6,3) layers with hcb topology. Further stacking of these layers on the basis of π–π interactions resulted in 3D supramolecular architectures. Additionally, the magnetic measurements of compounds **1** and **2** showed antiferromagnetic exchange interactions, while compound **3** exhibited ferromagnetic exchange interactions. This investigation provides some useful information to design and yield new coordination polymers with pyridine-type ligands and further enriches the magnetism of Co coordination polymers.

Supplementary Materials: The following are available online at http://www.mdpi.com/2073-4352/9/3/166/s1. Tables S1–S3: Selected bond distances and angles, Figures S1–S6: Structural information of compounds **1**–**3**, Figure S7–S9: 3D supramolecular architecture of compounds **1**–**3**, Figures S10–S13: PXRD data of compounds **1**–**3**, the ligands of H_2L_1 and H_2L_2, Figures S14–S16: IR of compounds **1**–**3**, Figure S17: Photographs of compounds **1**–**3**, Figure S18: SEM images of compounds **1**–**3**.

Author Contributions: X.Z. and X.G. conceived and designed the experiments; X.Z. performed the experiments; L.L. and Y.P. analyzed the data; Z.S. collected the data; X.T. supervised the work. All the authors contributed to the manuscript revision.

Funding: This work was supported by the Open Project of State Key Laboratory of Inorganic Synthesis and Preparation of Jilin University 2017−35, the Research Fund for the Doctoral Program of Weifang University (2016BS06), the Natural Science Foundation of Shandong Province of China (ZR2017MB056), and the National Natural Science Foundation Youth Fund (201802104).

Conflicts of Interest: The authors declare no conflict of interest.

References

1. Espallargas, G.M.; Coronado, E. Magnetic functionalities in MOFs: From the framework to the pore. *Chem. Soc. Rev.* **2018**, *47*, 533–557. [CrossRef] [PubMed]
2. Liang, H.X.; Jiao, X.L.; Li, C.; Chen, D.R. Flexible self-supported metal–organic framework mats with exceptionally high porosity for enhanced separation and catalysis. *J. Mater. Chem. A* **2018**, *6*, 334–341. [CrossRef]
3. Chughtai, A.H.; Ahmad, N.; Younus, H.A.; Laypkov, A.; Verpoort, F. Metal–organic frameworks: Versatile heterogeneous catalysts for efficient catalytic organic transformations. *Chem. Rev.* **2015**, *44*, 6804–6849. [CrossRef] [PubMed]
4. Liu, J.W.; Chen, L.F.; Cui, H.; Zhang, J.Y.; Zhang, L.; Su, C.Y. Applications of metal–organic frameworks in heterogeneous supramolecular catalysis. *Chem. Soc. Rev.* **2014**, *43*, 6011–6061. [CrossRef]
5. Hu, Z.C.; Deibert, B.G.; Li, J. Luminescent metal–organic frameworks for chemical sensing and explosive detection. *Chem. Soc. Rev.* **2014**, *43*, 5815–5840. [CrossRef] [PubMed]
6. Getman, R.B.; Bae, Y.S.; Wilmer, C.E.; Snurr, R.Q. Review and Analysis of Molecular Simulations of Methane, Hydrogen, and Acetylene Storage in Metal–Organic Frameworks. *Chem. Rev.* **2012**, *112*, 703–723. [CrossRef] [PubMed]
7. Li, J.R.; Sculley, J.; Zhou, H.C. Metal–Organic Frameworks for Separations. *Chem. Rev.* **2012**, *112*, 869–932. [CrossRef] [PubMed]
8. Cui, Y.J.; Yue, Y.F.; Qian, G.D.; Chen, B.L. Luminescent Functional Metal–Organic Frameworks. *Chem. Rev.* **2012**, *112*, 1126–1162. [CrossRef]
9. Corma, A.; García, H.; Llabrés i Xamena, F.X. Engineering Metal Organic Frameworks for Heterogeneous Catalysis. *Chem. Rev.* **2010**, *110*, 4606–4655. [CrossRef]
10. Li, B.Y.; Zhou, X.J.; Zhou, Q.; Li, G.H.; Hua, J.; Bi, Y.; Li, Y.J.; Shi, Z.; Feng, S.H. Design and construction of coordinationpolymers based on 2,2′-dinitro-4,4′-biphenyldicarboxylate and imidazole-basedligands: The effect of ligand length and metal ions. *CrystEngComm* **2011**, *13*, 4592–4598. [CrossRef]
11. Zhang, J.P.; Lin, Y.Y.; Zhang, W.X.; Chen, X.M. Temperature or Guest-Induced Drastic Single-Crystal-to-Single-Crystal Transformations of a Nanoporous Coordination Polymer. *J. Am. Chem. Soc.* **2005**, *127*, 14162–14163. [CrossRef] [PubMed]

12. Wu, Y.P.; Li, D.S.; Fu, F.; Dong, W.W.; Zhao, J.; Zou, K.; Wang, Y.Y. Stoichiometry of N-Donor Ligand Mediated Assembly in the ZnII-Hfipbb System: From a 2-Fold Interpenetrating Pillared-Network to Unique (3,4)-Connected Isomeric Nets. *Cryst. Growth Des.* **2011**, *11*, 3850–3857. [CrossRef]
13. Li, B.Y.; Zhang, Z.J.; Li, Y.; Yao, K.X.; Zhu, Y.H.; Deng, Z.Y.; Yang, F.; Zhou, X.J.; Li, G.H.; Wu, H.H.; et al. Enhanced Binding Affinity, Remarkable Selectivity, and High Capacity of CO_2 by Dual Functionalization of a rht-Type Metal-Organic Framework. *Angew. Chem. Int. Ed.* **2012**, *1*, 1412–1415. [CrossRef] [PubMed]
14. Yang, Y.; Zhang, X.M.; Ma, J.P.; Liu, Q.K.; Wang, P.; Dong, Y.B. Cu(I)-MOF: Naked-eye colorimetric sensor for humidity and formaldehyde in single-crystal-to-single-crystal fashion. *Chem. Commun.* **2014**, *50*, 1444–1446.
15. Xue, M.; Zhu, G.S.; Ding, H.; Wu, L.; Zhao, X.J.; Jin, Z.; Qiu, S.L. Six Three-Dimensional Metal–Organic Frameworks with (3,4)-, (4,5)-, and (3,4,5)-Connected Nets Based on Mixed Ligands: Synthesis, Structures, and Adsorption Properties. *Cryst. Growth Des.* **2009**, *9*, 1481–1488. [CrossRef]
16. Zhou, X.J.; Zhang, Z.J.; Li, B.Y.; Yang, F.; Peng, Y.; Li, G.H.; Shi, Z.; Feng, S.H.; Li, J. Two three-dimensional metal–organic frameworks constructed by thiazole-spaced pyridinecarboxylates exhibiting selective gassorption or antiferromagnetic coupling. *New J. Chem.* **2013**, *37*, 425–430. [CrossRef]
17. Zhou, X.J.; Li, B.Y.; Li, G.H.; Zhou, Q.; Shi, Z.; Feng, S.H. Synthesis, structures and luminescent properties of cadmium(II) metal organic frameworks based on 3-pyrid-4-ylbenzoic acid, 4-pyrid-4-ylbenzoic acid ligands. *CrystEngComm* **2012**, *14*, 4664–4669. [CrossRef]
18. Gao, Q.; Jiang, F.L.; Wu, M.Y.; Huang, Y.G.; Yuan, D.Q.; Wei, W.; Hong, M.C. Indium(III)-2,5-pyridine dicarboxylate complexes with mononuclear, 1D chain, 2D layer and 3D chiral frameworks. *CrystEngComm* **2009**, *11*, 918–926. [CrossRef]
19. Das, M.C.; Ghosh, S.K.; Sanudo, E.C.; Bharadwaj, P.K. Coordination polymers with pyridine-2,4,6-tricarboxylic acid and alkaline-earth/lanthanide/transition metals: Synthesis and X-ray structures. *Dalton Trans.* **2009**, 1644–1658. [CrossRef]
20. Sun, F.X.; Zhu, G.S. Solvent-directed synthesis of chiral and non-centrosymmetric metal-organic frameworks based on pyridine-3,5-dicarboxylate. *Inorg. Chem. Commun.* **2013**, *38*, 115–118. [CrossRef]
21. Liu, Y.T.; Du, Y.Q.; Wu, X.; Zheng, Z.P.; Lin, X.M.; Zhua, L.C.; Cai, Y.P. A series of lanthanide complexes based on pyridine-3,5-dicarboxylate and succinate ligands: Syntheses, structures and properties. *CrystEngComm* **2014**, *16*, 6797–6802. [CrossRef]
22. Wang, X.L.; Qin, C.; Wang, E.B.; Xu, L.; Su, Z.M. Synthesis, structure and luminescent properties of two three-dimensional d10 metal complexes constructed from pyridine-3,4-dicarboxylic acid with new network topologies. *J. Mol. Struct.* **2006**, *796*, 172–178. [CrossRef]
23. Lin, X.M.; Niu, J.L.; Wen, P.X.; Lu, Y.N.; Hu, L.; Zhang, D.L.; Cai, Y.P. From 1D to 3D lanthanide coordination polymers constructed with pyridine-3,5-dicarboxylic acid: Synthesis, crystal structures, and catalytic properties. *RSC Adv.* **2016**, *6*, 63425–63432. [CrossRef]
24. Yang, F.; Zhou, Q.; Zeng, G.; Li, G.H.; Gao, L.; Shi, Z.; Feng, S.H. Anion effects on the structures and magnetic properties of binuclear lanthanide single-molecule magnets. *Dalton Trans.* **2014**, *43*, 1238–1245. [CrossRef] [PubMed]
25. Li, S.D.; Lu, L.P.; Feng, S.S.; Zhu, M.L. Syntheses, structures, magnetic properties and luminescence of four coordination polymers based on an asymmetric semirigid tricarboxylate ligand. *J. Solid State Chem.* **2019**, *269*, 56–64. [CrossRef]
26. He, Y.P.; Tan, Y.X.; Wang, F.; Zhang, J. Microporous Zinc Tris [(4-carboxyl) phenylduryl] amine Framework with an Unusual Topological Net for Gas Storage and Separation. *Inorg. Chem.* **2012**, *51*, 1995–1997. [CrossRef] [PubMed]
27. Zhao, J.; Liu, B.; Wu, Y.P.; Bai, L.; Zhang, J.; Li, D.S. $[Co(H_2O)_6]^{2+}$ and H_3O^+ encapsulated in a unique 3D anionic Co(II) framework with hydrophilic hexagonal and circular channels. *CrystEngComm* **2015**, *17*, 7034–7037. [CrossRef]
28. Wang, J.C.; Ding, F.W.; Ma, J.P.; Liu, Q.K.; Cheng, J.Y.; Dong, Y.B. Co(II)-MOF: A Highly Efficient Organic Oxidation Catalyst with Open Metal Sites. *Inorg. Chem.* **2015**, *54*, 10865–10872. [CrossRef]
29. Chae, S.H.; Kim, H.C.; Lee, Y.S.; Huh, S.; Kim, S.J.; Kim, Y.; Lee, S.J. Thermally Robust 3-D Co-DpyDtolP-MOF with Hexagonally Oriented Micropores: Formation of Polyiodine Chains in a MOF Single Crystal. *Cryst. Growth Des.* **2015**, *15*, 268–277. [CrossRef]

30. Jin, J.; Gong, Y.Y.; Li, L.; Han, X.; Meng, Q.; Liu, Y.H.; Niu, S.Y. Spectroscopic properties of a series of Co(II) coordination polymers and the influence of Co(II) coordination environment on photoelectric property. *Spectrochim. Acta Part A* **2015**, *137*, 856–863. [CrossRef]
31. Murinzi, T.W.; Hosten, E.; Watkins, G.M. Synthesis and characterization of a cobalt-2,6-pyridinedicarboxylate MOF with potential application in electrochemical sensing. *Polyhedron* **2017**, *137*, 188–196. [CrossRef]
32. Gu, J.Z.; Liang, X.X.; Cai, Y.; Wu, J.; Shi, Z.F.; Kirillov, A.M. Hydrothermal assembly, structures, topologies, luminescence, and magnetism of a novel series of coordination polymers driven by a trifunctional nicotinicacid building block. *Dalton Trans.* **2017**, *46*, 10908–10925. [CrossRef] [PubMed]
33. Liu, X.B.; Xiao, Z.Y.; Huang, A.; Wang, W.; Zhang, L.L.; Wang, R.M.; Sun, D.F. Crystal structures, topological analysis and luminescence properties of three coordination polymers based on a semi-rigid ligand and N-donor ligand linkers. *New J. Chem.* **2016**, *40*, 5957–5965. [CrossRef]
34. Bo, Y.X.; Na, S.Y.; Yang, W.; Juan, Z.L.; Wei, L.Q. Synthesis, structure and luminescence properties of metal-organic frameworks based on benzo-bis(imidazole). *Sci. China Chem.* **2014**, *57*, 135–140.
35. O'Keeffe, M.; Peskov, M.A.; Ramsden, S.J.; Yaghi, O.M. The Reticular Chemistry Structure Resource (RCSR) Database of, and Symbols for, Crystal Nets. *Acc. Chem. Res.* **2008**, *41*, 1782–1789. [CrossRef]
36. Noh, T.H.; Lee, H.; Jang, J.; Jung, O.S. Organization and Energy Transfer of Fused Aromatic Hydrocarbon Guests within Anion-Confining Nanochannel MOFs. *Angew. Chem. Int. Ed.* **2015**, *54*, 9284–9288. [CrossRef]
37. Wang, C.C.; Yang, C.C.; Chung, W.C.; Lee, G.H.; Ho, M.L.; Yu, Y.C.; Chung, M.W.; Sheu, H.S.; Shih, C.H.; Cheng, K.Y.; et al. A New Coordination Polymer Exhibiting Unique 2D Hydrogen-Bonded $(H_2O)16$ Ring Formation and Water-Dependent Luminescence Properties. *Chem. A Eur. J.* **2011**, *17*, 9232–9241. [CrossRef]
38. Lupton, J.M.; Samuel, I.D.W.; Burn, P.L. Origin of spectral broadening in π-conjugated amorphous semiconductors. *Phys. Rev. B* **2002**, *66*, 155206. [CrossRef]
39. Akpinar, I.; Drout, R.J.; Islamoglu, J.; Kato, S.; Lyu, J.F.; Farha, O.K. Exploiting π–π Interactions to Design an Efficient Sorbent for Atrazine Removal from Water. *ACS Appl. Mater. Interfaces* **2019**, *11*, 6097–6103. [CrossRef]
40. Yao, R.X.; Cui, X.; Jia, X.X.; Zhang, F.Q.; Zhang, X.M. A Luminescent Zinc(II) Metal–Organic Framework (MOF) with Conjugated π-Electron Ligand for High Iodine Capture and Nitro-Explosive Detection. *Inorg. Chem.* **2016**, *55*, 9270–9275. [CrossRef]